Journal of Materials Science: Materials in Electronics
https://doi.org/10.1007/s10854-020-03007-4

Structural and Opto-electronic characterization of CuO thin films prepared by DC reactive magnetron sputtering

Xi Zeng[1] · Maria Zhukova[1] · Sébastien Faniel[1] · Joris Proost[2] · Denis Flandre[1]

Received: 12 October 2019 / Accepted: 29 January 2020

Abstract
P-type CuO thin films have been deposited and optimized for large-area photodetection applications by tuning the sputtering pressure and oxygen to argon gas ratio, considering both high-temperature sputtering and post-annealing. The obtained layers show tunable bandgaps from 1.30 to 2.04 eV and Urbach energies lower than 8 meV. Reliable Hall measurements reveal the inverse double logarithmic relationship between Hall mobility and carrier concentration. By setting the optimal sputtering pressure of 10 mTorr (O_2/Ar = 8/22 sccm) at the edge of oxidization and transition regimes, CuO with 1.64 eV bandgap reaches stable hole mobility of 34.2 cm^2V^{-1} s^{-1} and hole concentration of 3.92×10^{14} cm^{-3} after 250 °C post-annealing. Considering heating at 150 °C during the deposition, CuO with 1.63 eV bandgap also reaches stable record hole mobility of 113.7 cm^2V^{-1} s^{-1} and hole concentration of 1.39×10^{14} cm^{-3}.

1 Introduction

Photodetectors for instrumentation or communication applications mostly use Si, Ge or III–V technologies, toward high performance but limited device size (maximum a few mm^2). To achieve higher-sensitivity, lower-cost and larger-area photodetection over a few cm^2 in biomedical imaging and environmental applications [1], several novel materials, including MoS_2 [2, 3], $MoSe_2$ [4], SnS_2 [5], ZnO [6], perovskite [7], and graphene [1, 8], have been studied.

Copper oxide also appears a good candidate as large-area photodetection material. It is currently considered as one of the most promising p-type metal oxide semiconductors because of its abundance in the earth crust, low cost, nontoxicity, easy recyclability, stability in the air as well as high optical absorption and good charge transport properties [9, 10]. Copper oxide with three different phases (CuO, Cu_4O_3 and Cu_2O) can be obtained by varying the fabrication parameters. Compared to Cu_4O_3 and Cu_2O, *p*-type monoclinic structure CuO with lower tunable bandgap from 1.2 to 1.9 eV, higher optical absorption and more stable chemical performance, is more suitable to be used as the photo-absorption material in photodetector applications [10–12].

Several techniques have been considered in the synthesis of CuO, including thermal oxidation [13, 14], atomic layer deposition [15], ionic layer deposition [16], chemical bath deposition [17], sol–gel process [18], solution process [19], vapor–liquid-solid method [20], pulsed laser deposition [21], spin-coating [22], microwave-activated sputtering [23], magnetron sputtering [24, 25] etc. Among these techniques, DC reactive magnetron sputtering is an easy-controlled, low-cost and reliable technique in large-area industrial fabrication. The structural, physical, optical or electrical properties of CuO prepared by direct current (DC) reactive magnetron sputtering have been recently studied considering variations in oxygen partial pressure [26–32]. Radio frequency (RF) reactive magnetron sputtering is also considered in CuO deposition [33]. However, few researches focus on the overall fabrication, characterization and analysis of sputtered CuO thin films with the target of large-area photodetection applications. Therefore, sputtering and optimization of CuO thin films by tuning the sputtering parameters are necessary before the fabrication of high-performance large-area CuO-based photodetectors.

In this work, DC reactive magnetron sputtering is utilized to fabricate the copper oxide thin films under different

✉ Xi Zeng
xi.zeng@uclouvain.be

[1] Institute of Information and Communication Technologies, Electronics and Applied Mathematics, Université Catholique de Louvain, 1348 Louvain-la-Neuve, Belgium

[2] Institute of Mechanics, Materials and Civil Engineering, Université Catholique de Louvain, 1348 Louvain-la-Neuve, Belgium

Published online: 07 February 2020

sputtering parameters including sputtering pressure, oxygen to argon gas ratio and substrate temperature during sputtering. Furthermore, post-annealing is considered to boost the carrier mobility of CuO thin films. Full material, optical and electrical characterizations of the obtained CuO films have been carried out with the aim to obtain the best performing CuO with bandgap around 1.5 to 1.7 eV, carrier concentration around 10^{15} cm^{-3} and maximum carrier mobility. With such results, our CuO layers show a great potential to be utilized as the large-area photodetection material in the UV and near visible spectral range.

2 Experimental details

Soda lime glass (SLG) substrates with a size of 2.4 × 2.4 cm^2 were cleaned by acetone, methanol, iso-propanol and deionized water, and dried by nitrogen before the deposition of CuO thin films by direct current (DC) reactive magnetron sputtering (ATC Orion 5 Sputter System from AJA International [34]). The substrates fixed in the sample holder are positioned 122 mm away from the Cu target (99.999% purity) and rotated at 45 rpm under a vacuum base pressure of around 10^{-7} Torr. The total gas flow rate of Ar and O_2 was set to a constant value of 30 sccm under a sputtering pressure varied from 5 to 15 mTorr. All the samples were sputtered with a constant sputtering power of 50 W for 30 min, after a target cleaning of 5 min with Ar plasma and 3 min with Ar/O_2 plasma. Post-annealing was carried out in N_2 for 30 min at 250 and 450 °C. High-temperature sputtering at 150, 250 and 350 °C were also investigated.

After deposition, the material properties were analyzed by X-ray diffraction (XRD) with CuKα radiation (λ = 1.5418 Å), field-emission gun scan electron microscope (FEGSEM, Zeiss Ultra 55 field-emission gun), Raman Spectroscopy (LabRAM HR from Horiba Scientific) and Film Thickness Measurement System (Veeco Dektak 150). The optical properties were characterized by UV–VIS-IR spectrophotometer (Specord 200 PLUS from Analytic Jena) with illumination between 200 and 1100 nm. The electrical properties were measured by Hall Effect Measurement System (HMS3000) with gold probes as contacts under a permanent magnet field of 0.55 T and by 4 Point Probe Resistivity Measurement (Lucas-Signaton with SUM-Keithley 2400) at room temperature.

3 Results and discussion

3.1 Structural characterization

In order to determine the best copper oxide thin film for photodetector applications, discharge voltage (i.e. voltage between the chamber and the target, with the substrate floating) obtained on the SLG substrate is measured as a function of oxygen concentration varied from 3.33% (O_2/Ar = 1/29 sccm) to 66.67% (O_2/Ar = 20/10 sccm) in Fig. 1. In addition, different sputtering pressures of 5, 10 and 15 mTorr are investigated because the pressure can significantly influence the microstructure of the films. When increasing oxygen concentration in the sputtering chamber, the copper target is gradually oxidized and three regimes can be observed in Fig. 1, corresponding to the oxidization regime, transition regime and poisoned regime of copper oxide successively. Three phases of copper oxides including CuO, Cu_4O_3 and Cu_2O can be deposited in the oxidization regime. After fully oxidizing CuO, the discharge voltage gradually decreases in the transition regime until reaching the second plateau (poisoned regime), where the film is over-oxidized to form poor-quality copper oxide. The transition regime can be used to tune different qualities of CuO with various bandgaps, while the poisoned regime is not recommended [35].

A low sputtering pressure of 5mTorr at room temperature is set as the reference pressure to check the film quality in different regimes: O_2/Ar = 10/20 sccm in oxidization regime (O10 sample, 160 nm thickness), O_2/Ar = 15/15 sccm in transition regime (O15 sample, 65 nm), and O_2/Ar = 20/10 sccm in poisoned regime (O20 sample, 66 nm). In Fig. 2a, the XRD patterns show that CuO (JCPDS-45-0937) could be obtained from the edge of oxidization regime and transition regime to the poisoned regime. All as-deposited CuO feature the phase of tenorite CuO, and monoclinic crystal structure in the C2/c(15) space group. Moreover, the main peaks at 2θ = 32.5, 35.5,

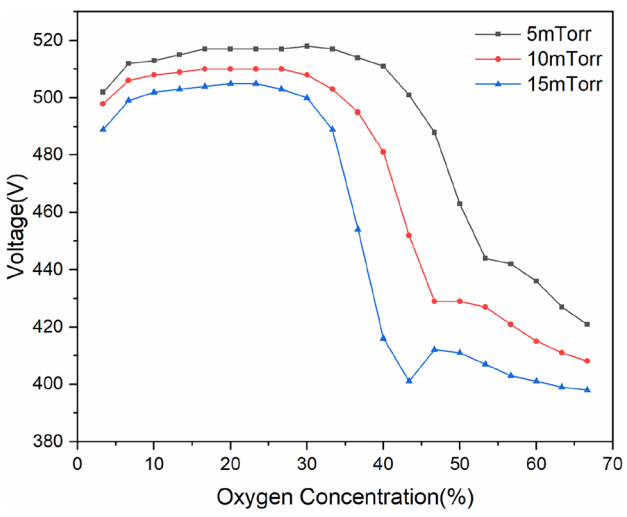

Fig. 1 Discharge voltage as a function of oxygen concentration in the sputtering chamber, with a constant sputtering power of 50 W and a constant total gas flow rate (O_2 + Ar) of 30 sccm at room temperature

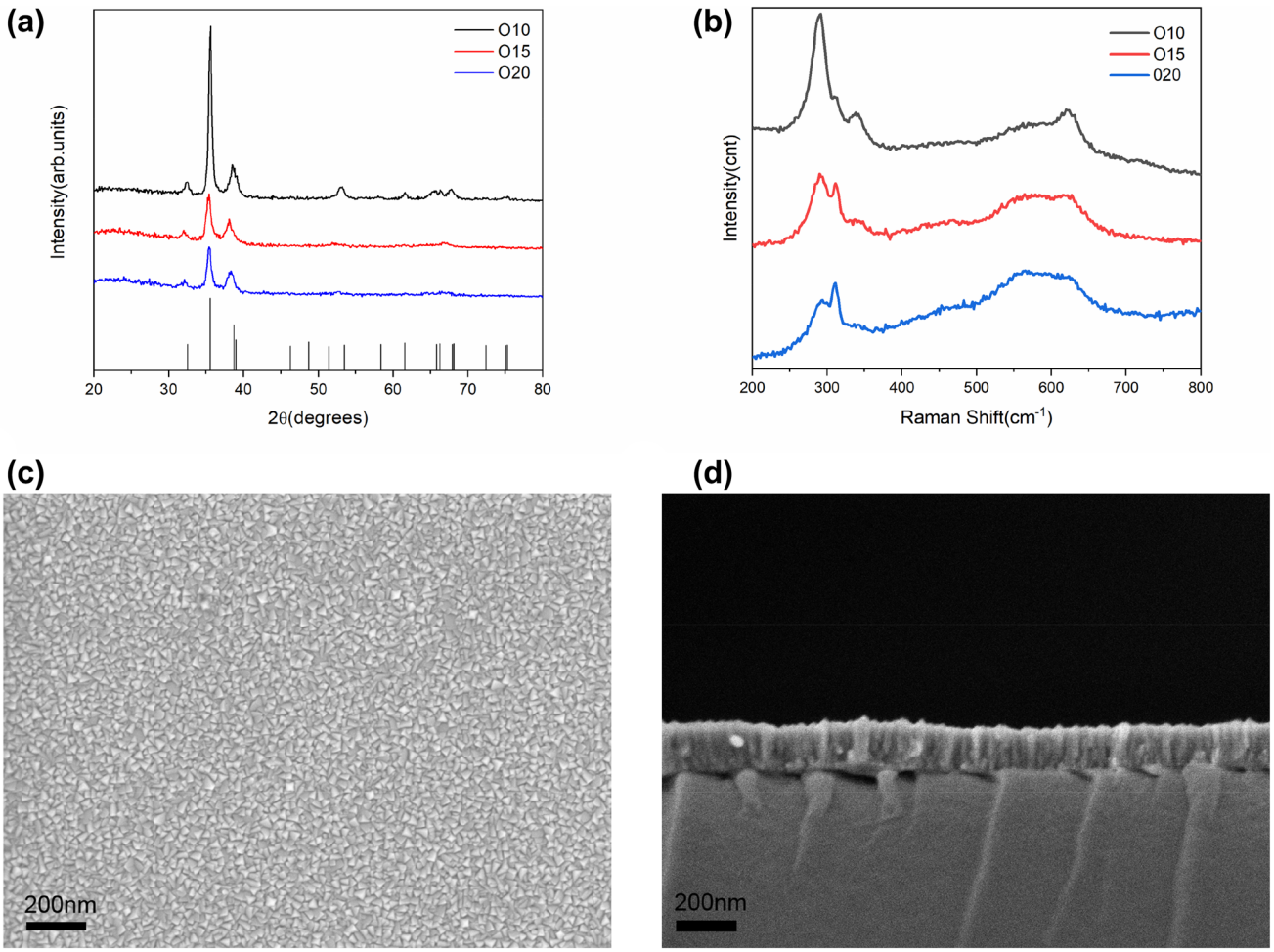

Fig. 2 **a** XRD patterns (JCPDS-45–0937) of O10 sample (O_2/Ar = 10/20 sccm), O15 sample (O_2/Ar = 15/15 sccm), O20 sample (O_2/Ar = 20/10 sccm) at 5 mTorr sputtering pressure; **b** Raman spectra of O10, O15, O20 samples at 5 mTorr at room temperature, by 514 nm radiation; **c** SEM Plane section view and **d** SEM cross section view of CuO deposited on SLG at 5 mTorr with 33% oxygen (O_2/Ar = 10/20 sccm)

38.7 are corresponding to the reflection planes of (− 110), (002) and (111) axes. The crystallite sizes for O10, O15 and O20 samples are 19.34 nm, 18.02 nm and 17.55 nm, respectively, as calculated by Debye-Scherer relation, $D = 0.94\lambda/\beta\cos\theta$, where λ is the X-ray wavelength, and β is the half width of maximum peak intensity [24].

In Fig. 2b, the Raman peaks of CuO lie around 288 cm^{-1} for the first A_g mode, 330 cm^{-1} for the second much weaker B_g mode and 621 cm^{-1} for the third broader B_g mode [36]. The crystalline size change would cause a slight change of CuO peaks. Raman peaks of O10 sample in Fig. 2b are 291, 343 and 623 cm^{-1}, which are consistent with the results in literature [36]. With the increase of oxygen concentration, the Raman peaks become weaker and blunter, which corresponds to the decreasing grain size as observed in the XRD results. For all Raman spectra, the peak at 310 cm^{-1} is observed, which corresponds to the peak of SLG substrate and can be neglected in further analysis. While increasing oxygen concentration, intensity increases in the Raman shift from 400 to 600 cm^{-1} could be observed due to the increase of CuO structural defects and the increase of amorphous phase fraction [37].

The SEM plain-view micrograph of O10 sample in Fig. 2c reveals a triangular grain structure of CuO and an estimated grain size of about 20 nm, which is consistent with the XRD result and similar to the CuO grain size of 22 nm in literature [24]. The SEM cross-sectional view of O10 sample in Fig. 2d shows a columnar growth of CuO from the glass surface to the top of CuO thin film. Meanwhile, no clear SEM graphs of the O15 and 020 samples could be obtained because of poor-quality CuO crystal structures and too much charge effect from the glass substrate. According to the structural characterizations, the best CuO thin film is the O10 sample, at the edge of oxidation and transition regimes, showing excellent morphological performance, larger grain size and less defects.

In order to obtain the best-studied copper oxide for large-area photodetection applications, copper oxide should be sputtered under the oxidation regime to avoid poor-quality CuO in transition and poisoned regimes. Therefore, in this work, oxygen to argon ratios are next set to 10/20, 8/22 and 7/23 sccm for 5, 10 and 15 mTorr sputtering pressure respectively, which corresponds to 5mTorr (O10), 10mTorr (O8) and 15mTorr (O7) samples at the edge of oxidation and transition regimes. In order to improve the quality of copper oxide thin film, we consider post-annealing at 250 and 450 °C for 30 min in N_2 as well as substrate heating at 150, 250, and 450 °C for 30 min during the sputtering. The thicknesses of all deposited samples on SLG substrates are listed in Table 1. Considering the constant sputtering time for all samples, the thickness of copper oxide thin film decreases gradually with the increase of annealing temperature and sputtering temperature. Meanwhile, the XRD and Raman measurements keep similar for all samples, which reveals a good grain growth of CuO.

3.2 Optical characterization

The reflectance spectra of copper oxide thin films sputtered under different pressures and different gas ratios with varied annealing and sputtering temperatures given in Table 1 are shown in Fig. 3. With the increase of incident wavelength, a hump could be observed near 400 nm for all samples because of the interferences related to the small thicknesses of the films. Besides, the valleys near the bandgaps are caused by the limiting absorption wavelength of copper oxides. The high reflectance in infrared regime is mainly caused by the back reflectance of the glass substrate. For the sputtering at room temperature, the reflectance of as-deposited samples keeps low at 6–26% for 5mTorr (O10), 5–27% for 10mTorr (O8), and 6–30% for 15mTorr (O7). With the increase of post-annealing or sputtering temperature, the reflectance of copper oxide film increases in the whole wavelength, which corresponds to the decrease of copper oxide thickness.

Next, the transmittance spectra of copper oxide thin films are given in Fig. 4. The average optical transmittance in the visible and near infrared region increases with increasing annealing temperature from 43.71 to 41.75% for 5mTorr (O10), 51.12 to 41.31% for 5mTorr (O10), and 54.96 to 45.76% for 5mTorr (O10), respectively. With the increase of sputtering temperature, the average transmittance of copper oxide films also decreases from 51.17% for 10mTorr (Room) to 41% for 10mTorr (350 °C). With the increase of incident wavelength, more incident photons are transmitted through the film, which corresponds to less excited charge carriers across the optical bandgap [38]. A hump near the limiting absorption wavelength of CuO is also found in transmittance spectra, which demonstrates the optical tuning properties of sputtering technique [24]. High transmittance in infrared regime exhibits high transparency of CuO for infrared light, which corresponds to no carrier excitation behavior for incident photon energy less than the bandgap. The transmittances of all samples reach stable values of around 60% in near infrared regime, while the transmittance humps observed around 850 nm in the samples of Fig. 4a are due to much lower reflectance caused in this range by a larger thickness of the CuO films compared to other samples. For the samples in Fig. 4a, transmittances decrease beyond 850 nm, towards 60%, that other samples also show around 1100 nm.

In Fig. 5, the absorption coefficients of copper oxide thin films in the spectral range from 320 to 1100 nm ($h\nu = 3.875–1.127$ eV) are calculated by utilizing the standard formula:

$$\alpha = \frac{1}{\text{th}} \ln\left(\frac{(1-R)^2}{T}\right) \tag{1}$$

where th is the film thickness, R and T are the reflectance and transmittance obtained in Figs. 3 and 4. The absorption coefficient α, which decreases with the increase of incident wavelength and with the decrease of incident light energy, can reach over 10^5 cm^{-1}. According to the relation:$d = \frac{1}{\alpha}$, where d is the light penetration depth, the incident light is absorbed by copper oxide near the surface, within less than 100 nm in the UV and near visible spectral region. In the far visible and infrared region, the films reveal very low absorption coefficient, which shows that copper oxide is almost transparent to the long-wavelength incident light

Table 1 Thicknesses of samples deposited on SLG substrates under varied sputtering pressures and oxygen concentrations, annealing temperatures and sputtering temperatures

Varied annealing temperatures	Room (nm)	250 °C (nm)	450 °C (nm)
5mTorr (O10)	160	148	140
10mTorr (O8)	120	114	96
15mTorr (O7)	90	80	60

Varied sputtering temperatures	Room (nm)	150 °C (nm)	250 °C (nm)	350 °C (nm)
10mTorr (O8)	120	110	100	95

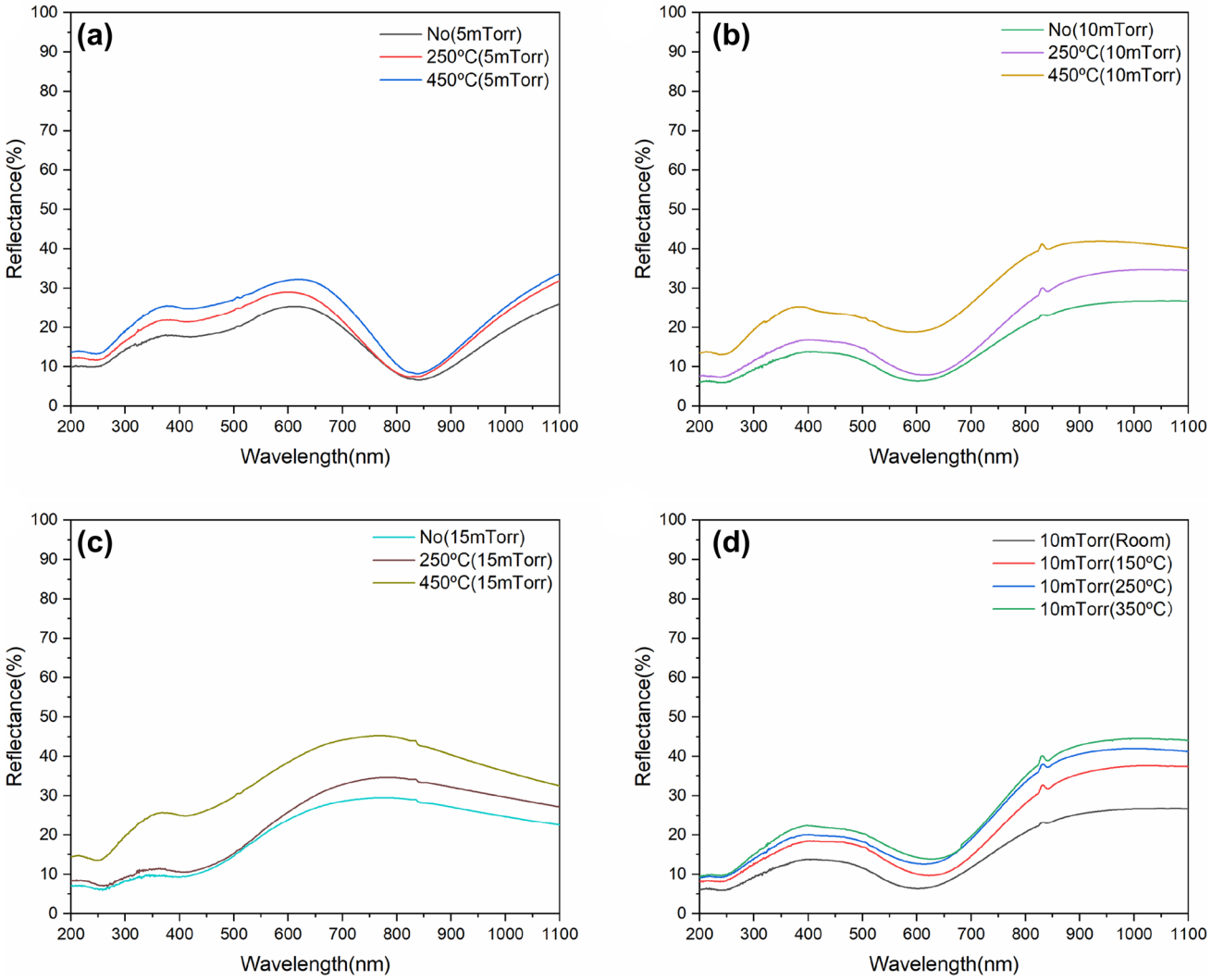

Fig. 3 Reflectance spectra of CuO thin films deposited under different post-annealing temperatures (250 and 450 °C) at **a** 5mTorr (O10); **b** 10mTorr (O8); **c** 15mTorr (O7); and **d** 10mTorr (O8) under different sputtering temperatures from 150 to 350 °C

and the incident light penetrates through the copper oxide with few photoexcitation. Low penetration depth of copper oxide in the UV and near visible spectral region allows the limitation of the copper oxide thickness in the photodetector applications to less than 100 nm.

The optical bandgaps of copper oxide thin films are calculated in Fig. 6 by using the Tauc relation:

$$(\alpha h\nu)^n = A\left(h\nu - E_g\right) \tag{2}$$

where α is the absorption coefficient, h is the Plank constant, ν is the incident light frequency, n is the transition probability of material, and A is a constant value related to the material [29]. The magnitude of n is equal to 2 or 1/2 for direct allowed or indirect allowed transitions respectively. The general type of CuO bandgap stays controversial, but CuO with lower bandgap (1–1.5 eV) utilizes indirect transition in long-wavelength photodetection [19]. Conversely, copper oxide with higher bandgap targeting short-wavelength photodetection is considered as direct transition semiconductor, which corresponds to the n magnitude of 2 [16, 24]. Considering the target on short-wavelength photodetection, the magnitude of 2 is used to extract the linear portion of plot, in which the x-intercept value of the linear portion is equal to the bandgap value. Considering the increase of sputtering pressure and the decrease of oxygen concentration for the sputtering at room temperature, the bandgap of CuO increases from 1.39 to 2.04 eV with the decrease of film thickness from 160 to 90 nm. With the increase of annealing temperature or sputtering temperature, the bandgap of CuO increases gradually while the CuO film thickness decreases gradually.

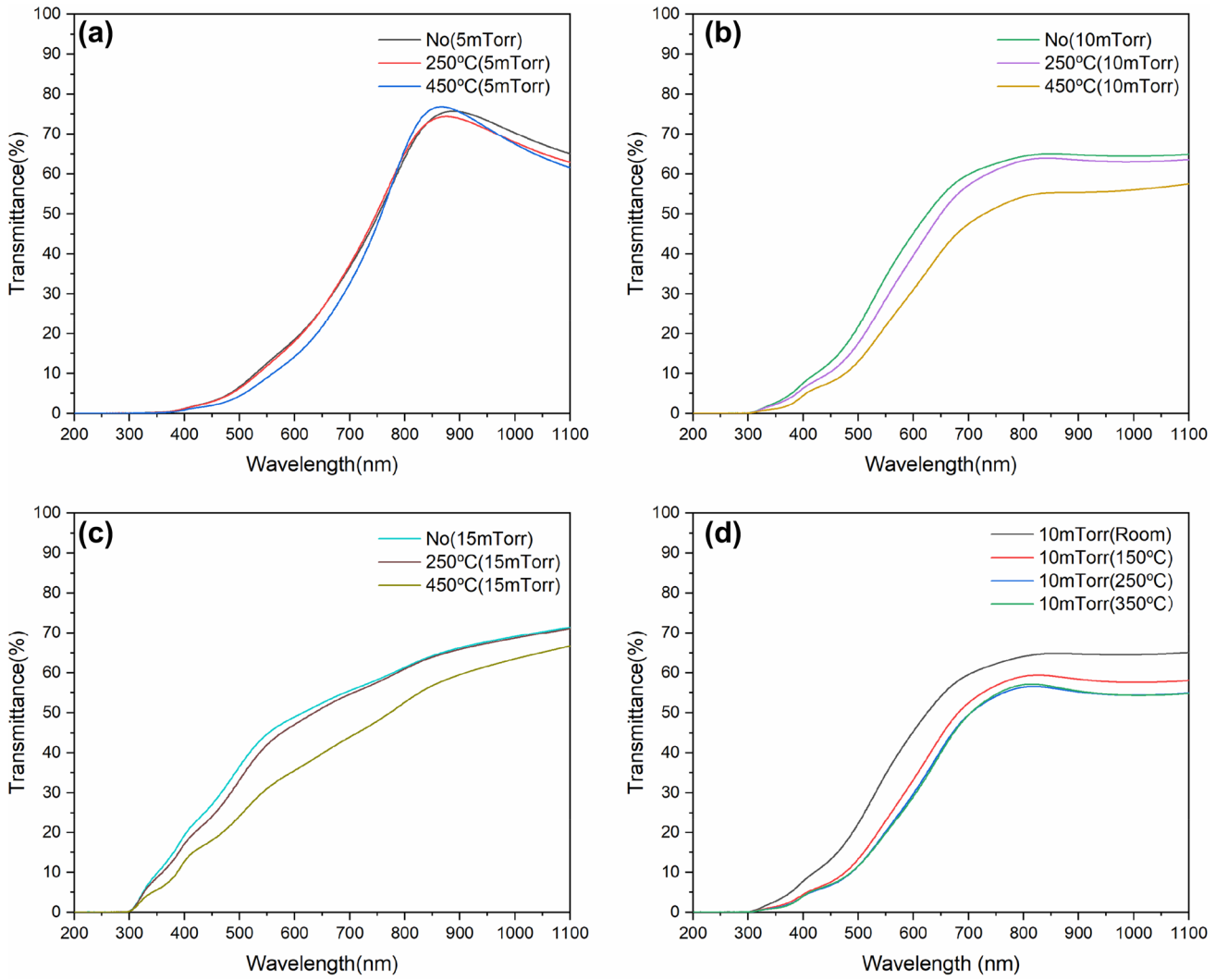

Fig. 4 Transmittance spectra of CuO thin films deposited under different post-annealing temperatures (250 and 450 °C) at **a** 5mTorr (O10); **b** 10mTorr (O8); **c** 15mTorr (O7); and **d** 10mTorr (O8) under different sputtering temperatures from 150 to 350 °C

In order to fabricate a photodetector-valuable thin film, the most suitable bandgaps could be obtained under the sputtering pressure of 10mTorr (O_2/Ar = 8/22 sccm). In this sputtering condition, the CuO bandgap increases from 1.6 to 1.72 eV with increasing annealing temperature, while the thickness decreases from 120 to 96 nm. Meanwhile, the CuO bandgap increases from 1.6 to 1.68 eV with increasing sputtering temperature, while the thickness decreases from 120 to 95 nm.

In semiconductors and insulators, the absorption edge below the optical bandgap is considered as Urbach tail, which is a key parameter related to the defect condition in semiconductors. The Urbach tails of copper oxide thin films are calculated in Fig. 7 by the Urbach's rule:

$$\alpha(h\nu, T) = \alpha_0 e^{\left[\frac{h\nu - E_0}{E_U(T)}\right]} \tag{3}$$

where α_0 and E_0 are the characteristic parameters of materials, and $E_U(T)$ is the Urbach energy, which is reverse to the absorption edge slope $E_U^{-1} = \frac{\Delta(\ln \alpha)}{\Delta(h\nu)}$ [39]. Urbach energy is highly related to the measurement temperature, so in this work all the measurements are done at room temperature. For all the samples, the Urbach energies are less than 8 meV, which reveals a very low defect density for all the CuO samples. The bandgaps and Urbach energies for all deposited samples are listed in Table 2.

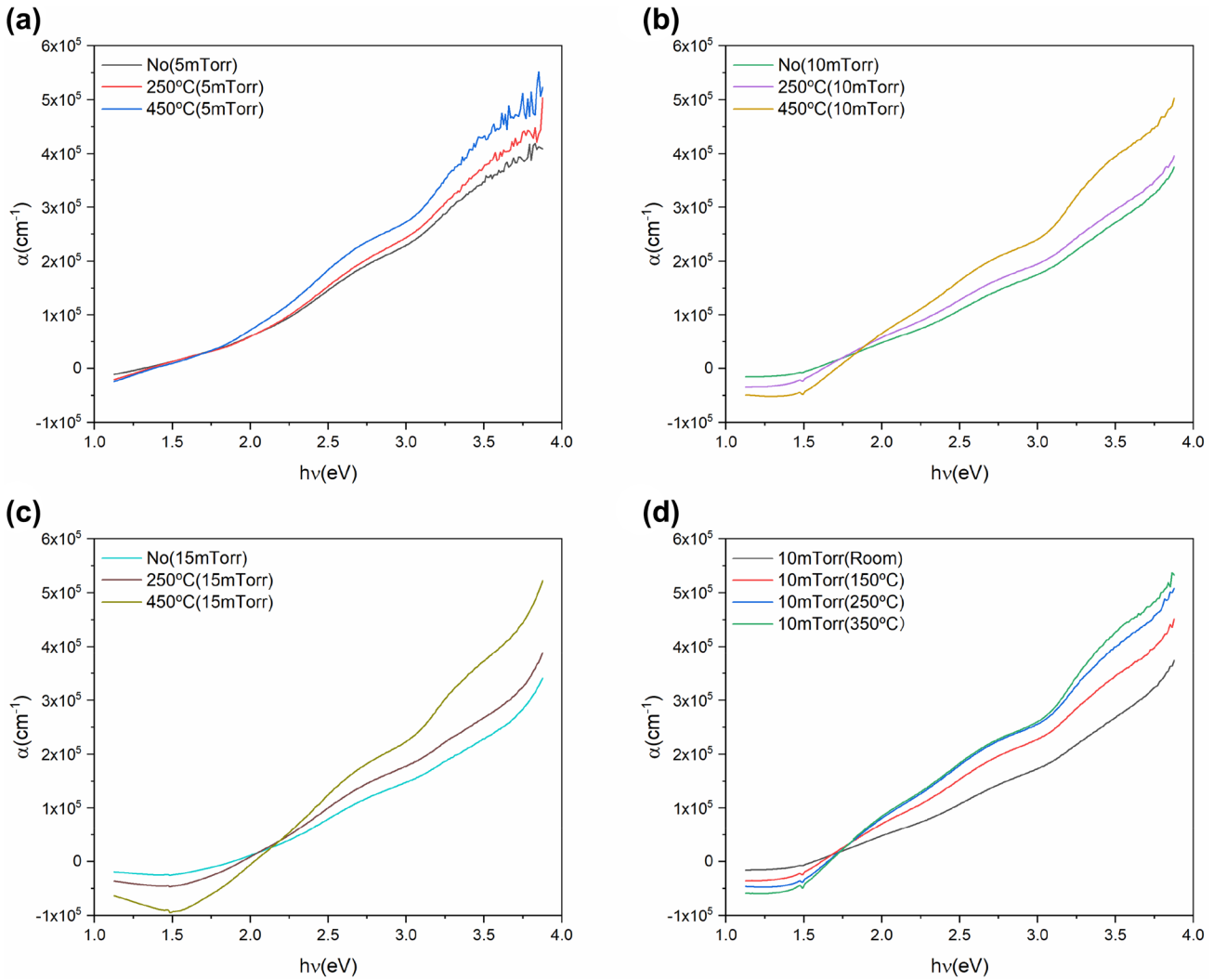

Fig. 5 Absorption coefficient spectra of of CuO thin films deposited under different post-annealing temperatures (250 and 450 °C) at **a** 5mTorr (O10); **b** 10mTorr (O8); **c** 15mTorr (O7); and **d** 10mTorr (O8) under different sputtering temperatures from 150 to 350 °C

3.3 Electrical characterization

Hall measurements using van der Pauw method have been carried out (Fig. 8) to obtain Hall mobility and carrier concentration of deposited copper oxide thin films compared to the reference CuO considering the gas ratio, sputtering pressure, sputtering temperature and annealing temperature variations. Sheet resistances characterized by both Hall Effect measurement and four-point probe measurement (Fig. 9) are also important parameters to check the accuracy of Hall measurement and quality of copper oxide. Considering that no doping was done in the fabrication process, the measured Hall mobility (μ), carrier concentration (N_p) and sheet resistance (R_s) come from the intrinsic doping of copper oxide. For the measurements of 15mTorr as-deposited and 250 °C-annealed samples, the sheet resistances are too high according to 4-probe measurements, that show a big difference compared to the results of Hall measurements. Therefore, these two samples are highly insulating, which causes a very low measured voltage and thus an unreliable Hall mobility. For all other samples, the sheet resistances for both Hall and four-point probe measurements keep close, which enables their correct Hall characterization. The reliable Hall measurements reveal the p-type conductivity of all these copper oxide samples. When setting both x and y-axis in logarithmic scale, the hole mobility reveals an increasing linear tendency with decreasing hole concentration, which fits the formula of $\log\mu + 0.495\log N_p = 8.988$. To realize stable high-performance copper oxide thin films for photodetector applications, several points could be extracted from the Hall measurement results. For room-temperature sputtering at 10mTorr, from one sample to another, Hall mobility could vary from 143.3 cm^2V^{-1} s^{-1}

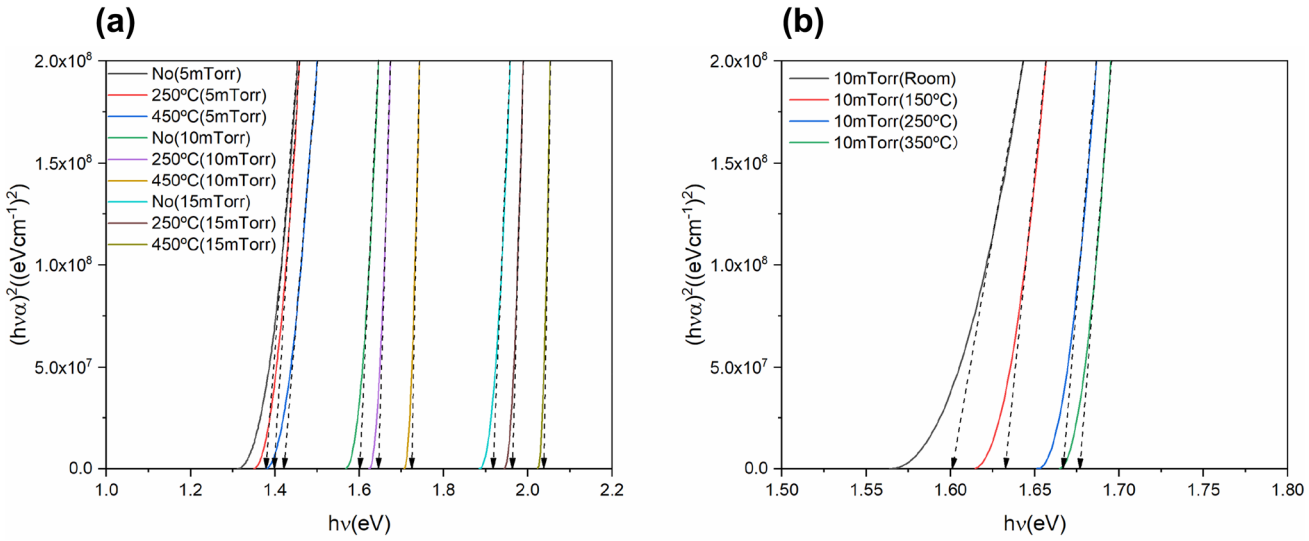

Fig. 6 Tauc plots of CuO thin films deposited at **a** 5mTorr(O10), 10mTorr(O8) and 15mTorr(O7) with varied post-annealing temperatures; **b** 10mTorr(O8) with varied sputtering temperatures

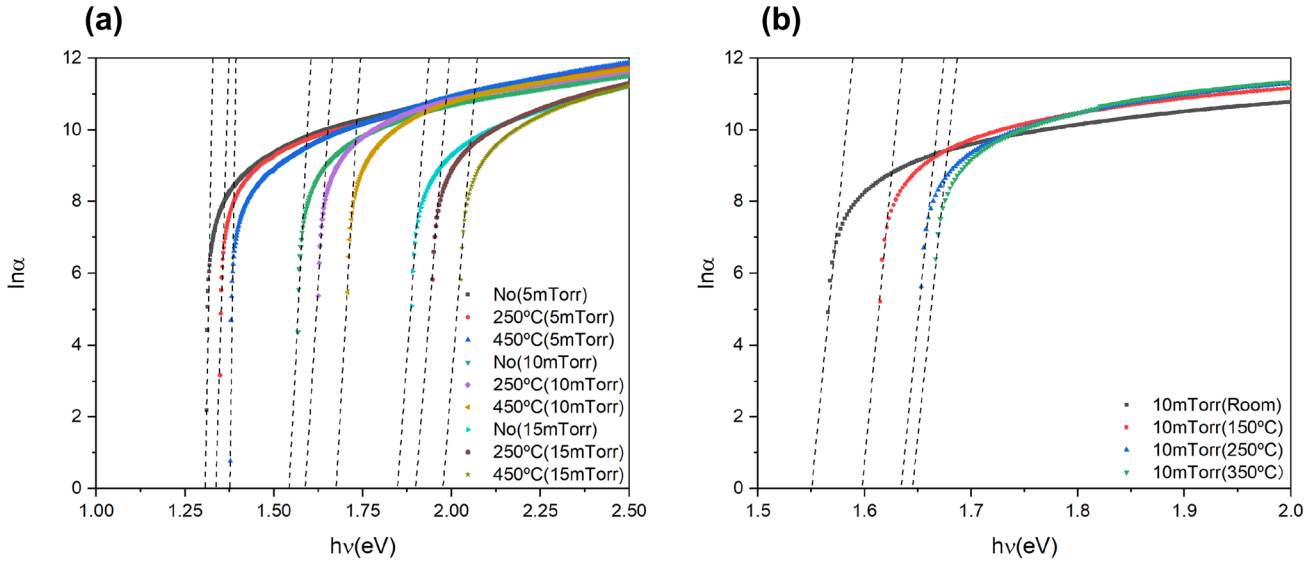

Fig. 7 Urbach tails plots of copper oxide thin films deposited at **a** 5mTorr (O10), 10mTorr (O8) and 15mTorr (O7) with varied post-annealing temperatures; **b** 10mTorr (O8) with varied sputtering temperatures

Table 2 Bandgaps and Urbach energies (in parenthesis) of samples deposited on SLG substrates under varied sputtering pressures and oxygen concentrations, annealing temperatures and sputtering temperatures

Varied annealing temperatures	Room	250 °C	450 °C
5mTorr(O10)	1.39 eV (2.1 meV)	1.4 eV (2.3 meV)	1.42 eV (1.4 meV)
10mTorr(O8)	1.60 eV (4.3 meV)	1.64 eV (5.1 meV)	1.72 eV (5.4 meV)
15mTorr(O7)	1.92 eV (6.7 meV)	1.96 eV (7.1 meV)	2.04 eV (7.1 meV)

Varied sputtering temperatures	Room	150 °C	250 °C	350 °C
10mTorr(O8)	1.60 eV (2.9 meV)	1.63 eV (2.5 meV)	1.67 eV (4.0 meV)	1.67 eV (4.0 meV)

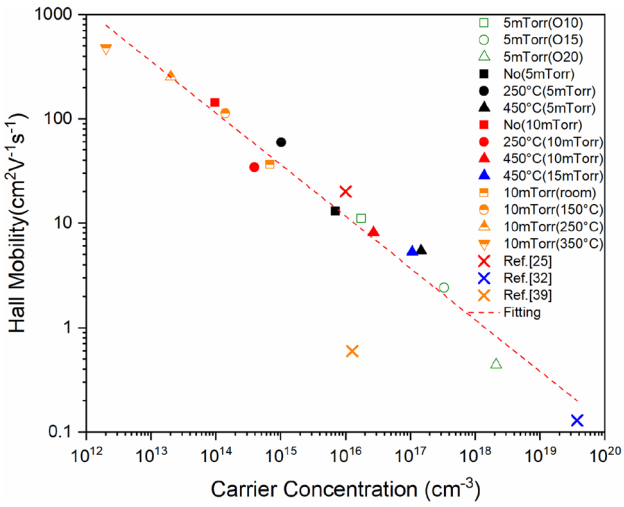

Fig. 8 Reliably-extracted Hall mobility of deposited and reference p-type CuO thin films versus carrier concentration

(with hole concentration $N_p = 9.64 \times 10^{13}$ cm^{-3}) to 36.33 cm^{2}V^{-1} s^{-1} ($N_p = 6.76 \times 10^{14}$ cm^{-3}), corresponding to the varying sheet resistance R_s from 3.6×10^7 to 2.12×10^7 Ω·sq^{-1}. Hence, these samples are hardly reproducible and furthermore reveal lower mobility values several days after the deposition. Post-annealing at 250 °C has shown the ability to stabilize Hall measurements and to improve the film quality, yielding reproducible hole mobility of 34.2 cm^{2}V^{-1} s^{-1} ($N_p = 3.92 \times 10^{14}$ cm^{-3}) for sample sputtered at 10mTorr ($R_s = 3.58 \times 10^7$ Ω·sq^{-1}). Heating at 150 °C during deposition can also stabilize the hole mobility to 113.7 cm^{2}V^{-1} s^{-1} ($N_p = 1.39 \times 10^{14}$ cm^{-3}) for sample sputtered at 10mTorr ($R_s = 3.43 \times 10^7$ Ω·sq^{-1}). High-temperature sputtering and post-annealing obviously improve the adatom mobility of the atoms on the substrate and thus improve the quality of the final CuO films, which results in the boost and stabilization of hole carrier mobility [40, 41]. These enhanced hole mobilities lead to improved conductivities of CuO films and thus a higher output current, with dark carrier concentrations adequate for future photodetector applications [42].

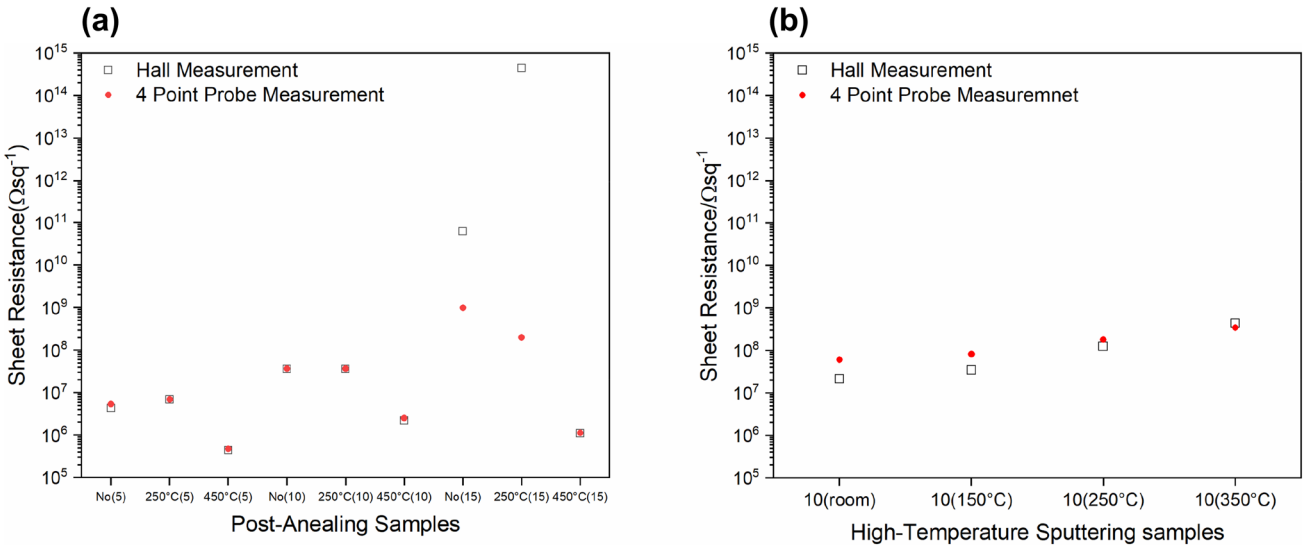

Fig. 9 Sheet resistance of CuO thin films deposited at **a** 5mTorr (O10), 10mTorr (O8) and 15mTorr (O7) with varied post-annealing temperatures; **b** 10mTorr (O8) with varied sputtering temperatures

Table 3 Opto-Electronic properties of improved CuO thin films (Sample A sputtered at 10mTorr and post-annealed at 250 °C, Sample B sputtered at 10mTorr and 150 °C) compared to best results in literature

Samples	Bandgap(eV)	Absorption coefficient (cm^{-1}, 320–500 nm)	Urbach energy(meV)	Hole mobility(cm^{2}V^{-1} s^{-1})	Hole concentration(cm^{-3})	Sheet resistance(Ω·sq^{-1})
A	1.64	$(1.25–4) \times 10^5$	5.1	34.2	3.92×10^{14}	3.58×10^7
B	1.63	$(1.5–4.5) \times 10^5$	2.5	113.7	1.39×10^{14}	3.43×10^7
Reference [24]	1.43	$(1–2) \times 10^5$	/	20	10^{16}	/

By tuning the sputtering parameters, considering high-temperature sputtering or post-annealing, the optical and electrical properties of CuO thin films in Table 3 are obviously improved compared to the previously reported best DC room-temperature sputtered CuO (with 100 nm thickness) for photodetector fabrication [24]. CuO films obtained in the present work feature twice the absorption coefficient than in previous works, which results in a shallower optical absorption depth in CuO surface and thus promises faster photo-response in future applications. Few studies have reported the calculation of Urbach energy for DC sputtered CuO. For RF-sputtered CuO with a bandgap of 1.7 eV, the calculated Urbach energy is 167 meV in [43], which is much higher than in this work. For most of the previously reported DC sputtered CuO films, the hole mobility stays very low, less than 1 cm^2V^{-1} s^{-1} [31, 44]. The best reported CuO film to date reaches a hole mobility of 20 cm^2V^{-1} s^{-1} [24], which is still much lower than the values in our work. Meanwhile, the hole concentration and sheet resistance still keep in adequate value regions for photodetectors. In this work, CuO thin films with a bandgap of about 1.6 eV, high absorption coefficient and very low Urbach energy reach record hole mobilities of 34.2 cm^2V^{-1} s^{-1} after 250 °C post-annealing and 113.7 cm^2V^{-1} s^{-1} when sputtered at 150 °C, which are both the highest stable mobilities reported till now.

4 Conclusions

Detailed structural, optical and electrical characterizations have been performed to obtain the best p-type CuO thin films, as deposited and improved by tuning the DC reactive magnetron sputtering conditions on soda lime glass substrate for large-area photodetection applications in UV and near visible spectral range. The curves of sputtering discharge voltage to oxygen concentration show three different sputtering regimes of copper oxide, from which the best CuO quality is obtained at the edge of oxidization and transition regimes, as demonstrated by XRD, SEM and Raman analyses.

After extracting the best oxygen concentration at different sputtering pressures of 5, 10 and 15mTorr, high-temperature sputtering from 150 to 350 °C and post-annealing at 250 °C and 450 °C are both considered to improve the opto-electronic quality of CuO. By measuring the reflectance and transmittance with the UV–VIS-IR spectrophotometer, the calculated absorption coefficient can reach over 10^5 cm^{-1} in UV and near visible light spectral range, which reveals the possibility to reduce the CuO thickness to less than 100 nm. These copper oxide films achieve tunable bandgap from 1.30 to 2.04 eV and Urbach energies lower than 8 meV, which reveals a low defect density of sputtered copper oxides. Reliable Hall measurements reveal the inverse double logarithmic variation of Hall mobility with carrier concentration, which can be used to choose proper copper oxide film for specific applications.

In conclusion, our best room-temperature sputtered CuO (10mTorr, O_2/Ar = 8/22 sccm) thin films have achieved suitable $E_g = 1.6$ eV, and $\mu_p = 143.3$ cm^2V^{-1} s^{-1} or 36.33 cm^2V^{-1} s^{-1}, but not repeatable several days after deposition. Post-annealing at 250 °C can stabilize the hole mobility to 34.2 cm^2V^{-1} s^{-1} (with $E_g = 1.64$ eV, $N_p = 3.92 \times 10^{14}$ cm^{-3}, $R_s = 3.58 \times 10^7$ $\Omega \cdot sq^{-1}$). Heating at 150 °C during the deposition can also stabilize the hole mobility to 113.7 cm^2V^{-1} s^{-1} (with $E_g = 1.63$ eV, $N_p = 1.39 \times 10^{14}$ cm^{-3}, $R_s = 3.43 \times 10^7$ $\Omega \cdot sq^{-1}$). These two mobilities are both the highest reported values till now. These *p*-type CuO films with suitable bandgaps, very low Urbach energies, high hole mobilities, proper hole concentrations and sheet resistances are highly suitable to be utilized as the large-area photodetection material in the UV and near visible spectral range for the further research of photodiodes or photodetectors.

Acknowledgements This work is financially supported by China Scholarship Council and Université Catholique de Louvain Co-Funding Fellowship (No. CSC201806130158).

Compliance with ethical standards

Conflict of interest The authors declare that they have no conflicts of interest.

References

1. F.H. Koppens, T. Mueller, P. Avouris, A.C. Ferrari, M.S. Vitiello, M. Polini, Nat. Nanotechnol. **9**, 780 (2014)
2. O. Lopez-Sanchez, D. Lembke, M. Kayci, A. Radenovic, A. Kis, Nat. Nanotechnol. **8**, 497 (2013)
3. Z.P. Ling, R. Yang, J.W. Chai, S.J. Wang, W.S. Leong, Y. Tong, D. Lei, Q. Zhou, X. Gong, D.Z. Chi, K.W. Ang, Opt. Express **23**, 13580 (2015)
4. J. Xia, X. Huang, L.Z. Liu, M. Wang, L. Wang, B. Huang, D.D. Zhu, J.J. Li, C.Z. Gu, X.M. Meng, Nanoscale **6**, 8949 (2014)
5. J. Xia, D. Zhu, L. Wang, B. Huang, X. Huang, X.-M. Meng, Adv. Funct. Mater. **25**, 4255 (2015)
6. K. Sun, Y. Jing, N. Park, C. Li, Y. Bando, D. Wang, J. Am. Chem. Soc. **132**, 15465 (2010)
7. M.I. Saidaminov, V. Adinolfi, R. Comin, A.L. Abdelhady, W. Peng, I. Dursun, M. Yuan, S. Hoogland, E.H. Sargent, O.M. Bakr, Nat. Commun. **6**, 8724 (2015)
8. Y. Liu, F. Wang, X. Wang, X. Wang, E. Flahaut, X. Liu, Y. Li, X. Wang, Y. Xu, Y. Shi, R. Zhang, Nat. Commun. **6**, 8589 (2015)
9. H.J. Song, M.H. Seo, K.W. Choi, M.S. Jo, J.Y. Yoo, J.B. Yoon, Sci. Rep. **9**, 7334 (2019)
10. S. Masudy-Panah, R. Siavash Moakhar, C.S. Chua, H.R. Tan, T.I. Wong, D. Chi, G.K. Dalapati, ACS Appl. Mater. Interfaces **8**, 1206 (2016)

11. D. Wu, Q. Zhang, M. Tao, Phys. Rev. B **73**, 235206 (2006)
12. F. Gao, X.J. Liu, J.S. Zhang, M.Z. Song, N. Li, J. Appl. Phys **111**, 084507 (2012)
13. J. Liang, N. Kishi, T. Soga, T. Jimbo, M. Ahmed, Thin Solid Films **520**, 2679 (2012)
14. X. Zhang, D. Zhang, X. Ni, H. Zheng, Solid State Electron. **52**, 245 (2008)
15. T.S. Tripathi, I. Terasaki, M. Karppinen, J. Phys. Condens. Matter **28**, 475801 (2016)
16. Y. Akaltun, Thin Solid Films **594**, 30 (2015)
17. J. Sultana, S. Paul, A. Karmakar, G.K. Dalapati, S. Chattopadhyay, J. Mater. Sci. **29**, 12878 (2018)
18. S. Lee, W.Y. Lee, B. Jang, T. Kim, J.H. Bae, K. Cho, S. Kim, J. Jang, IEEE Electron. Dev. Lett. **39**, 47 (2018)
19. T. DIxit, A. Tripathi, K.L. Ganapathi, I.A. Palani, M.S. Ramachandra Rao, V. Singh, IEEE Electron. Dev. Lett. **40**, 255 (2019)
20. J. Sultana, A. Das, A. Das, N.R. Saha, A. Karmakar, S. Chattopadhyay, Thin Solid Films **612**, 331 (2016)
21. Z. Hubička, M. Zlámal, M. Čada, M. Kment, J. Krýsa, Catal. Today **328**, 29 (2019)
22. A. Nalbant, Ö. Ertek, I. Okur, Mater. Sci. Eng. **178**, 368 (2013)
23. Y. Alajlani, F. Placido, A. Barlow, H.O. Chu, S. Song, S. Ur Rahman, R. De Bold, D. Gibson, Vacuum **144**, 217 (2017)
24. H.S. Kim, M. Patel, P. Yadav, J. Kim, A. Sohn, D.W. Kim, Appl. Phys. Lett. **109**, 101902 (2016)
25. L. Radjehi, A. Djelloul, M. Bououdina, R. Siab, W. Tebib, Appl. Phys. A **124**, 723 (2018)
26. H.C. Lu, C.L. Chu, C.Y. Lai, Y.H. Wang, Thin Solid Films **517**, 4408 (2009)
27. D. Tahir, S. Tougaard, J. Phys. Condens. Matter **24**, 175002 (2012)
28. Y. Wang, S. Lany, J. Ghanbaja, Y. Fagot-Revurat, Y.P. Chen, F. Soldera, D. Horwat, F. Mücklich, J.F. Pierson, Phys. Rev. B **94**, 245418 (2016)
29. W. Zheng, Y. Chen, X. Peng, K. Zhong, Y. Lin, Z. Huang, Materials (Basel). **11**, 1253 (2018)
30. N.W. Sangwaranatee, N. Sangwaranatee, M. Horprathum, C. Chananonnawathorn, E. Sustini, Mater. Today Proc. **5**, 15198 (2018)
31. S. Sai Guru Srinivasan, B. Govardhanan, P. Aabel, M. Ashok, M.C. Santhosh Kumar, Sol. Energy **187**, 368 (2019)
32. N. Sangwaranatee, C. Chananonnawathorn, M. Horprathum, Mater. Today Proc. **5**, 13896 (2018)
33. Ş. Korkmaz, B. Geçici, S.D. Korkmaz, R. Mohammadigharehbagh, S. Pat, S. Özen, V. Şenay, H.H. Yudar, Vacuum **131**, 142 (2016)
34. S. Michotte, J. Proost, Sol. Energy Mater. Sol. Cells **98**, 253 (2012)
35. J. Proost, F. Henry, R. Tuyaerts, S. Michotte, J. Appl. Phys. **120**, 075308 (2016)
36. J.F. Xu, W. Ji, Z.X. Shen, W.S. Li, S.H. Tang, X.R. Ye, D.Z. Jia, X.Q. Xin, J. Raman Spectrosc. **30**, 413 (1999)
37. V.S. Levitskii, V.I. Shapovalov, A.E. Komlev, A.V. Zav'yalov, V.V. Vit'ko, A.A Komlev, E.S. Shutova, Tech. Phys. Lett. **41**, 1094 (2015)
38. A.S. Reddy, H.H. Park, V.S. Reddy, K.V.S. Reddy, N.S. Sarma, S. Kaleemulla, S. Uthanna, P.S. Reddy, Mater. Chem. Phys. **110**, 397 (2008)
39. I. Studenyak, M. Kranj, M. Kurik, Int. J. Opt. Appl. **4**, 76 (2014)
40. B. Giroire, M. Ali Ahmad, G. Aubert, L. Teule-Gay, D. Michau, J.J. Watkins, C. Aymonier, A. Poulon-Quintin, Thin Solid Films **643**, 53 (2017)
41. S. Masudy-Panah, R. Siavash Moakhar, C.S. Chua, A. Kushwaha, T.I. Wong, G.K. Dalapati, RSC Adv. **6**, 29383 (2016)
42. M. Zhukova, R. Kotipalli, O. Poncelet, L. Samain, L. Fourdrinier, D. Flandre, Optimization of optoelectrical properties of DC magnetron sputtered Cu2ZnSnS4 absorber layer (in E-MRS (European Materials Research Society) 2019-Spring Meeting). https://hdl.handle.net/2078.1/218948. Accessed 17 Dec 2019
43. J. Kaur, R. Singh, Surf. Rev. Lett. **25**, 1950029 (2018)
44. R.D. Prabu, S. Valanarasu, I. Kulandaisamy, V. Ganesh, M. Shkir, A. Kathalingam, J. Mater. Sci. **28**, 6754 (2017)